Landslide Susceptibility Assessment Using GIS and RS In the Havran River Basin (Balikesir-TURKEY)

Hasan OZDEMIR* Huseyin TUROGLU*

**Istanbul University, Geography Department, Ordu Cad. No: 196, 34459, Laleli, Istanbul-TURKEY*
e-mail: ozdemirh@istanbul.edu.tr, turogluh@istanbul.edu.tr

In this study we assess landslide susceptibility of Havran river basin using Geographical Information Systems (GIS), Remote Sensing (RS) data and the statistical index method. Landslide locations were interpreted from topographic maps and verified with field observations. The collected data was combined in a spatial database using GIS and RS. Lineament, NDVI and Land use/cover data of the basin were extracted from Landsat ETM+ and Spot XS satellite images. Other contributing factors of elevation, slope, aspect, curvature, lithology, distance to roads, rainfall and soil data of the basin were also included. A GIS-based assessment process was constructed using these eleven factors and a statistical index method was used to produce a map of susceptibility. The results of the analysis were verified using the original landslide location data. The comparison between the predicted result and the actual distribution of landslides showed a high consistency.

Keywords: Landslide susceptibility mapping, Statistical index method, Geographical information system, Remote sensing, Havran River basin.

1. Introduction

In more than 10 years different methods and techniques for evaluating landslide occurrence have been developed and proposed worldwide (Hansen, 1984; Varnes, 1984; Hutchinson, 1995; Crozier, 1995). These methods include inventory mapping (direct approach) and a set of indirect, quantitative methods, namely the knowledge-based (index), statistical (data-driven) and deterministic approaches (Carrara et al., 1998). Quantitative methods rely on observed relationships between controlling factors and landslides (Guzzetti et al. 1999). Statistical analysis in quantitative methods are used to obtain predictions of the mass-movement from a number of parameter maps (Yin and Yan, 1988; Gupta and Joshi, 1990; Lee et al., 2002; Ayalew et al., 2004; Carrara et al., 1991; Chung and Fabbri, 1999). They can be categorized into two subgroups according to their data analysis methods: bivariate and multivariate (Soeters and van Westen, 1996). The bivariate models consider each individual thematic map in terms of landslide distribution and can be easily implemented in GIS (van Westen 1997). Mapping past and recent slope movements, together with the identification and mapping of the conditioning or preparatory factors of slope instability, are key components for predicting future landslides (Carrara et al., 1998). Generally, the purpose of landslide susceptibility mapping is to highlight the regional distribution of potentially unstable slopes based on a detailed study of the contributing factors (Ayalew et al., 2004).

Since susceptibility mapping involves the handling and interpreting of a large amount of data, the use of GIS is very important. One advantage of assessing landslide susceptibility using GIS is the speed at which calculation can be performed. Additionally, complex techniques requiring a large number of map crossings and table calculations are feasible. Furthermore, RS has an important role in assessing the susceptibility of landslides. Mantovani et al. (1996) review the use of RS techniques for landslide studies and hazard zonation in Europe. This study reveals that remote sensing data are mostly used in preparation of some predisposing

factors for the assessment. So far, RS data have played a minor role in landslide investigations because of their limited resolution and the small size of landslide. Using topographical maps and field surveys, 84 landslides were determined in the study area. In order to assess the susceptibility in the area we used the statistical index method (van Westen, 1997) to qualitatively define the weight values. However, many different methods exist for the calculation of weight values.

2. Study Area

The Havran river basin is situated between the coordinates 494530 – 530806 Y and 4365088 - 4395802 X coordinate (UTM, ED 50, Zone 35 N) in the western part of the Balikesir district, western Turkey. With a perimeter of 138.8 km and covering an area of about 570 km^2 (Fig. 1), the elevation of the basin changes between 0-1290 m. The Havran River flows in a west to east direction through the basin.

Geologically, the study area consists of four main types of lithological units: metamorphic basement rocks of Paleozoic-Mesozoic (schists, metagrabbros, amphibolities, phyllites, recrystallized limestone; granitic plutons of Upper Oligosen-Lower Miocene; Ayvacık volcanics of Lower- Middle Miocene (intermediate lavas and pyroclastic rocks) and alluvium of Quaternary (pebble, sand, silt and clay).

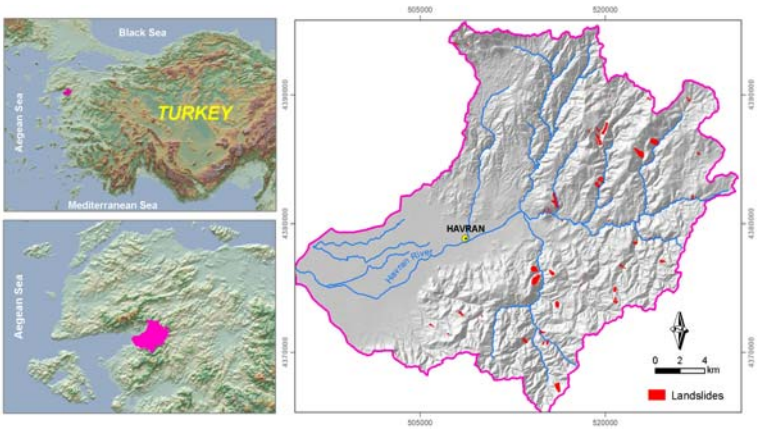

Figure 1: Location of study area and spatial distribution of landslides.

A Mediterranean climate dominates the study area with annual rainfall of 665 mm usually received during the months of November, December and January. The hottest month is July with an extreme maximum temperature of 41.3 ^{o}C. February is coldest month with an extreme minimum temperature of -6.3 ^{o}C.

The natural vegetation of the area comprises of pine tree (*Pinus brutia, Pinus nigra*) and some species of oak (*Querqus*) and maquis.

In the area, a total of 84 landslides have been determined from topographic maps and field surveys (Table 1, Fig. 1). All the landslides were classified into five types which are rotational slides, rock fall, debris flow, earth flow and topple (Table 1, Fig. 2). Some statistical properties of landslides are given in Table 1. Rotational movements represent 42% of the total landslides. They have the highest area with 73.3% (2979800 m^2) of the total landslide area. Rock falls represent 23.8% of the total movements and cover a total area of 21.1%. Debris flow, earth flow and topple have less area compared the first two types (Table 1). According to Zezere (2002), different types of landslides have neither the same magnitude nor equal damaging potential. Furthermore, technical strategies to mitigate land sliding also depend on landslide typology. These are additional reasons to discriminate between different types of slope movements when assessing landslide susceptibility and hazard. However in this case,

for the statistical analysis, landslide typology has not been mentioned due to the low number of landslides.

Table 1: Some statistical properties of landslides.

Types	No	% of Total	Area Min. (m^2)	Area Max. (m^2)	Total Area (m^2)	% of Total Area
Rotational Slide	42	50	590	338519	2979800	73.3
Rock Fall	20	23.8	1567	262427	857093	21.1
Debris Flow	15	17.8	641	45677	183800	4.6
Earth Flow	4	4.8	4350	10985	28671	0.7
Topple	3	3.6	3301	3887	10560	0.3
Total	**84**	**100**	**590**	**338519**	**4059924**	**100**

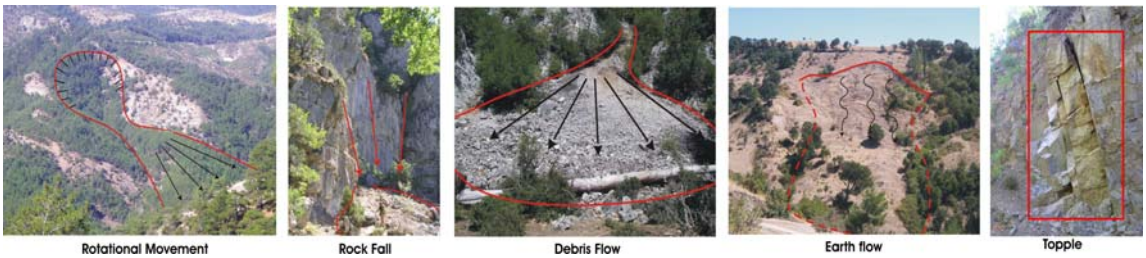

Figure 2: Examples of landslide types in the area (Photos by H. Ozdemir).

3. Data Collection and Database Construction

The construction of a cartographic database, comprising of the eleven maps used for landslide susceptibility assessment, was based on three different tasks: 1) digitizing, editing and analyzing of analog maps, 2) visual interpretation and classification of the satellite images, and 3) detailed field surveying (Fig. 3).

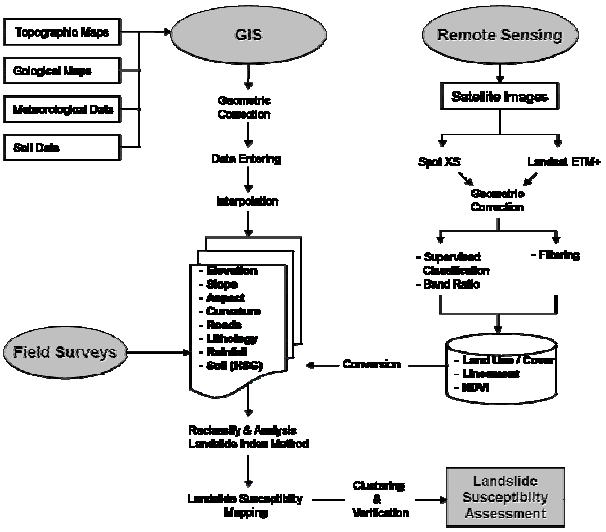

Figure 3: Flowchart of general methodology.

Topographical maps scaled 1:25000 was registered in the UTM projection plane (ED 50 Zone 35 N) and digitized in 10 m contour interval. The digital elevation model (DEM) was created from 10 m contour lines by a linear interpolation. Some layers were produced using the DEM, including slope angle, aspect and surface curvature on the basis of a moving 3x3 cell window. These criteria are proven to be predisposing factors for landslide activity. A pixel size of 10 m (100 m^2) was adapted to the DEM layer as well as the other parameters presented in Table 2.

Visual interpretation based on filtered image products, band ratio and supervised classification was the main techniques applied in the analysis of the RS data. Finally, some predisposing factors were prepared for susceptibility assessment using RS techniques.

The slope angle represents the gravitational force component and as such regulates mobilization vectors within a hill slope (Catani et al., 2005). It is therefore one of the most important driving parameters in landslide analysis. Derived from DEM, the slope angle layer

was classified into 5 classes (Table 2, Fig. 4) in order to more accurately represent site conditions. The aspect layer, also based on the the DEM, represents the angle between the the Geographic North and horizontal plain for a certain point and is classified by 8 major orientations (N, NE, E, SE, S, SW, W, NW) with the addition of flat areas. The transverse slope profile is an important variable that controls the superficial and subsurface hydrological regime of the slope (Zezere et al., 2004).

Table 2: Attribute data of parameters for susceptibility.

ID	Parameter Subclasses	∑Pix	Pix. No in Landslides	Density in Subclass	Indeks MethodWi
	Elevation				
1	0-250	2111377	4617	0.00219	-1.19018
2	250-500	1682408	22299	0.01325	0.60992
3	500-750	1623388	11803	0.00727	0.00968
4	750-1000	259327	2141	0.00826	0.13734
5	1000-1290	27244	243	0.00892	0.21421
	Curvature				
1	-0.39- (-0.01) Concave	704698	7386	0.01048	0.37539
2	(-0.01)-0.006 Strait	3759078	22823	0.00607	-0.17072
3	0.006-0.34 Convex	1239967	10894	0.00879	0.19953
	Lithology				
1	Tufe	15723	15	0.00095	-2.02537
2	Alluvium	989814	20	0.00002	-5.88610
3	Permien Olistolite	9647	0	0	
4	Granitic Pluton	387308	874	0.00226	-1.15872
5	Metagrovacs	626052	384	0.00061	-2.46838
6	Andesite and Tufe	2233032	24172	0.01082	0.40732
7	Alluvium Old	11443	0	0	
8	Neogen Sediment	367997	880	0.00239	-1.10279
9	Epimetamophise	149456	262	0.00175	-1.41447
10	Hornfles, Granotit	24343	0	0	
11	Limestone	224558	8463	0.03769	1.65531
12	Conglomerate	113447	1596	0.01407	0.66996
13	Dasite and Riolite	495875	3950	0.00797	0.10160
14	Poligenic Aglomerate	55397	487	0.00879	0.19953
	Slope (º)				
1	0-2	1242894	471	0.00038	-2.94167
2	2-15	1900495	12825	0.00675	-0.06454
3	15-25	1742484	13876	0.00796	0.10035
4	25-45	812712	12970	0.01596	0.79600
5	45-<	5158	961	0.18631	3.25333
	Aspect				
1	Flat (-1)	378238	237	0.00063	-2.43612
2	N (337.5-22.5)	614889	4916	0.00799	0.10411
3	NE (22.5-67.5)	439101	5783	0.01317	0.60386
4	E (67.5-112.5)	492395	7713	0.01566	0.77703
5	SE (112.5-157.5)	620659	8238	0.01327	0.61142
6	S (157.5-202.5)	578782	2913	0.00503	-0.35866
7	SW (202.5-247.5)	715914	2311	0.00323	-0.80160
8	W (247.5-292.5)	921288	3931	0.00427	-0.52247
9	NW (292.5-337.5)	942478	5061	0.00537	-0.29325
	Land Use/Cover				
1	Forest	2027098	25667	0.01267	0.56516
2	Iron mine	3392	0	0	
3	Agricultural Area	280656	21	0.00007	-4.63334
4	Maquis Area	793343	7124	0.00898	0.22092
5	Grass Area	243237	931	0.00383	-0.63122
6	Olive agriculture	852366	2344	0.00275	-0.96248
7	Settlement- Barren land	1499762	5006	0.00334	-0.76811
	NDVI				
1	-0.56-0.067	1471161	4478	0.00304	-0.86222
2	0.067-0.28	2001613	10931	0.00546	-0.27663
3	0.28-0.79	2228462	25694	0.01153	0.47087
	Rainfall				
1	581-704	1571100	0	0	
2	7704-837	1550400	15147	0.00977	0.30524
3	837-963	1320700	13806	0.01045	0.37252
4	963-1133	1118200	11288	0.01009	0.33746
5	1133-1429	142900	862	0.00603	-0.17733
	Distance to Lineament				
1	500	2546719	21474	0.00843	0.15772
2	1000	1493490	11770	0.00788	0.09025
3	1500	704122	4779	0.00679	-0.05863
4	2000	333655	1141	0.00342	-0.74444
5	2000<	626106	1939	0.00310	-0.84268
	Distance to Roads				
1	50	1375704	7910	0.00575	-0.22488
2	100	1114109	6653	0.00597	-0.18733
3	150	867875	5779	0.00666	-0.07796
4	200	657163	4944	0.00752	0.04349
5	200<	1689241	15817	0.00936	0.26236
	Soils (HSG)				
1	A	25068	0	0	
2	B	229059	0	0	
3	C	846496	86	0.00010	-4.27667
4	D	4602840	41017	0.00891	0.21309

Profile curvature represents the rate of change of slope for each cell in the direction of dipping (Ayalev et al., 2004). Profile curvature is divided by concave, convex and flat topographic surfaces. A positive curvature indicates that the surface is upwardly convex at that cell. A negative curvature indicates that the surface is upwardly concave at that cell. A value of zero indicates that the surface is relatively flat (Table 2).

Lithology was obtained from the geological map of the region (1:100000). The lithology is a fundamental instability factor in landslide analysis. The geological boundaries of the 14 lithological units (Table 2, Fig. 4) were verified and validated through fieldworks.

Road maps were obtained from topographical maps of the basin. Most landslides occurred on cut slopes or embankments alongside roads in mountainous areas. The construction of the main and secondary roads on steep slopes can be considered as the most important causative factor in the basin. In this study, a 50 m buffer (25+25) was applied to all types of roads based on field work observation. Areas in excess of 200 m above the road cut were not considered in the study (Table 2, Fig. 4).

Land use/cover greatly influences slope behaviour at every scale. In this study land use/cover map was obtained from Spot XS (2005) satellite images in conjunction with supervised classification and field works.

Land use/cover was classified in 7 class units which are forest area, iron mine, agricultural area, maquis area, grass area, olive field, and settlement – barren land (Table 2, Fig. 4).

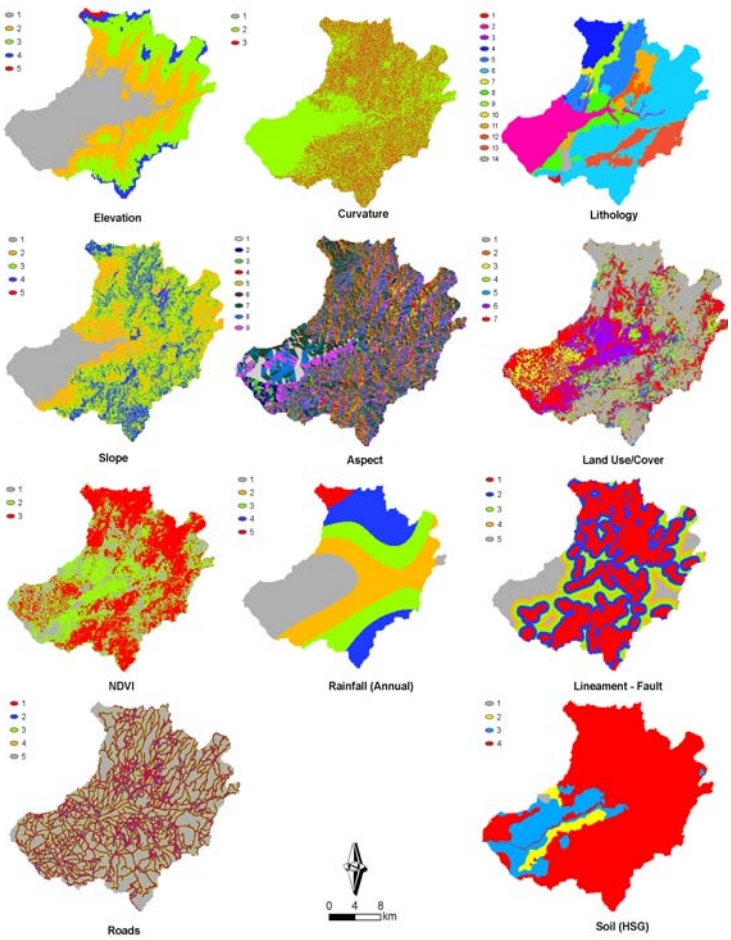

Figure 4: Parameter maps for landslide susceptibility.

Tectonic activity is differentiated with elevation range in the study area. Ozdemir, (2007) determined that tectonic variations are notable at 250 m intervals and therefore the range of elevation used in this study was 0-250, 250-500, 500-750, 750-1000 and 1000-1290 m (Table 2, Fig. 4)

Soil data was obtained from GDRS (General Director of Rural Services) in 1:25000 scales. Based on their hydrologic properties for water conditions and infiltration capacity, four units were classified. A indicates that the soil has high infiltration rates and low runoff potential whereas D indicates that the soil has very slow infiltration rates and high runoff potential. B and C units are close to A and D respectively (Table 2, Fig. 4).

NDVI (Normalized Difference Vegetation Index) data was obtained from Spot XS satellite images of the area. NDVI represents the vegetation cover and it is an index derived from reflectance measurements in the red and near infrared portions of the electromagnetic spectrum. This index describes the relative amount of active, green photosynthetic biomass present at the time the image was captured. NDVI was described in three subclasses which are dense vegetation, sparse vegetation and non vegetated areas (Table 2, Fig. 4).

A lineament map was created using 4, 5, 7 bands of Landsat ETM+ dated 2000 (Akhir et al., 1997; Voldai, 1995; Suzen et al., 1998). A Sobel directional filter was applied to the bands. Using fault lines obtained from geological maps of the area and the lineament, a 500 m (250 m+250 m) buffer was used to determine effect area. Distances in excess of 2000 m from the lineament were not considered in the study (Table 2, Fig. 4).

As rainfall is one of the triggering factors for landslide activity in the area, rainfall data was obtained from meteorological stations located near the basin. Using interpolation techniques an annual rainfall map was created for the entire basin. Natural break classification was applied to rainfall data (Table 2, Fig. 4).

4. Landslide Susceptibility Assessment and Validation

The applied statistical index method for the susceptibility assessment is based on a frequency analysis. This method simply defines the importance of a parameter subclass on landslide occurrence according to the spatial distribution of pixel of the considered parameter in relation to the landslide pixels. A standardization of the density values can be obtained by relating them to the overall density in the entire area. In this study the landslide density for each class is divided by the landslide density in for the entire map. The natural logarithm is used to give negative weights when the landslide density is lower than normal and positive when it is higher than normal (Van Wasten, 1997). By combining eleven maps of weight-values, a susceptibility map was created. According to the description, W_i is expressed as in following equation:

$$Wi = \ln \frac{Densclas}{Densmap} = \ln \left(\frac{\frac{Npix(S_i)}{Npix(N_i)}}{\frac{\sum Npix(S_i)}{\sum Npix(N_i)}} \right)$$

Where,
W_i= the weight given to a certain parameter class (e.g. lithology, or a slope class)
Densclas= the landslide density within the parameter class.
Densmap= the landslide density within the entire map.
$Npix(S_i)$= number of pixels, which contain landslides, in a certain parameter class.
$Noix(N_i)$= total number of pixels in a certain parameter class.

W_i values were calculated according to the pixel values tabulated in Table 2. The result of the calculation is given in Fig. 5a as non-classified. Final values of pixels are changing between -23.46 (low susceptibility) to 8.71 (high susceptibility). Classification of the final map into different susceptibility classes is very difficult. For this purpose, some authors use different kinds of techniques such as expert opinion, standard deviation, natural break, quantiles, equal interval etc. In this study, we considered cluster analysis based on iterative minimum distance of each pixel in five classes (Forgy, 1965) using SAGA GIS software (Fig. 6).

As is shown in Fig. 5b the five categories correspond to five relative scales of landslide susceptibility, namely none (or extremely low), very low, low, medium and high. In order to validate the results of the susceptibility assessment, the same landslide data set was used. Interpretation of Fig. 6a and b allow the identification of the following susceptibility classes:

I) The high susceptibility class includes 2 114 866 pixels (the largest susceptibility values that cover 37.22 % of study area) and 81.15% of the area of landslides;
II) The medium susceptibility class includes 1 882 317 pixels (33.13% of the study area) and includes 17.94% of landslides.
III) The low susceptibility class includes 636 979 pixels (11.21% of the study area) and includes 0.89% of landslides.
IV) The very low susceptibility class includes 438 928 pixels (7.72% of the study area) and includes 0.03% of landslides.
V) The extremely low susceptibility class includes 609 147 pixels (10.72% of the study area) with no landslides located in this area (0.00%).

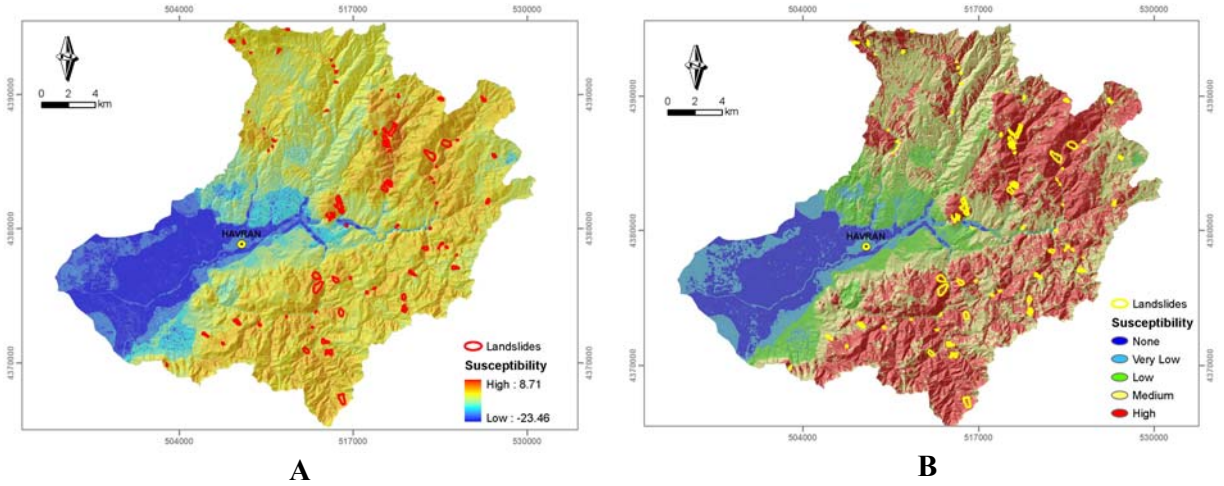

Figure 5: A) Non-classified landslide susceptibility map of Havran River basin B) Landslide susceptibility map of Havran River basin, classified according to minimum distance clustering method.

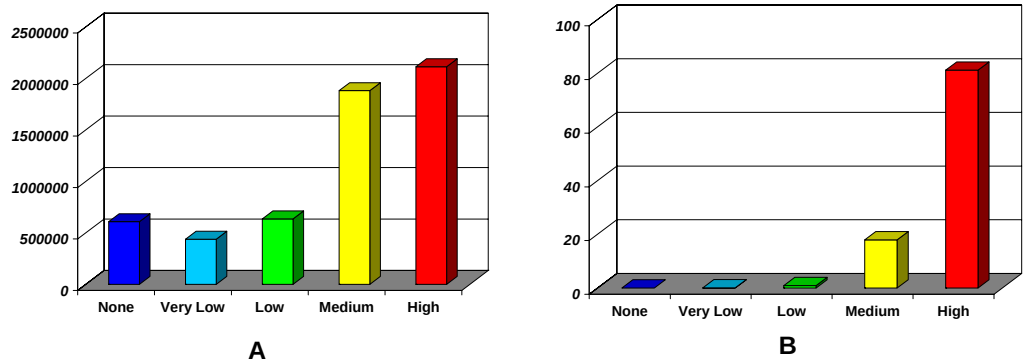

Figure 6: A) Distribution of susceptibility classes B) Percentage of landslide distribution in susceptibility classes.

5. Conclusion

The spatial distribution of landslides is a result of the interaction of many parameters. To create an accurate susceptibility map, proper parameters must be used. In this study eleven parameters namely, elevation, curvature, lithology, slope, aspect, land use/cover, NDVI, rainfall, lineament, roads and soil were considered. To create some parameters RS techniques were used. A method called statistical index method was used to extract the weight of each parameter. This method pointed out the importance of lithology and slope parameters above others, on landslide occurrence. The results of the entire analysis and evaluation allowed us to divide the study area into five zones of susceptibility, namely none or extremely low (10.72%), very low (7.72%), low (11.21%), medium (33.13%) and high (37.22%). Validation of the results, using same landslide data set, showed that the high susceptible zone includes 81.15% of landslide areas. All these studies have been done on a basin scale as it allows us to determine general probable landslide areas. In order to obtain a more precise result for use on a local scale a deterministic approach should be applied.

6. Acknowledgement

This work was supported by the Research Found of Istanbul University. Project number: T-583/17032005. Authors thank to Deanne Bird for her help.

7. References

Ayalew, L., Yamagishi, H., Ugawa, N., 2004. Landslide susceptibility mapping using GIS-based weighted linear combination, the case in Tsugawa area of Agano River, Niigata Prefecture, Japan. Landslides 1, 73–81.

Akhir, J.M., Abdullah, I., 1997. Geological Application of Landsat TM Imagery: Mapping and Analysis of Lineament in NW Peninsula Malaysia, www.gisdevelopment.net

Aleotti P., Chowdhury R., 1999, Landslide hazard assessment: summary review and new perspectives. Bull Eng Geol Environ 58:21–44

Carrara, A., Cardinali, M., Detti, R., Guzzetti, F., Pasqui, V., Reichenbach, P., 1991. GIS techniques and statistical models in evaluating landslide hazard. Earth Surface Processes and Landforms 16, 427–445.

Carrara, A., Guzzetti, F., Cardinali, M., and Reichenbach, P., 1998. Current limitations in modeling landslide hazard. In Buccianti, A., Nardi, G., and Potenza, R. (Eds.), Proceedings of IAMG'98, 195–203,.

Catani, F., Casagli, N., Righini, G., Menduni, G., 2005. Landslide hazard and risk mapping at the catchment scale in the Armo River basin, Landslides, 2: 329-342.

Chung C-JF., Fabbri AG., 1999. Probabilistic prediction models for landslide hazard mapping. Photo Eng Remote Sens 65:1389–1399

Crozier, M. J., 1995. Landslide hazard assessment, theme report. In Bell (Ed.), Landslides, Proceedings of the 6th International Symposium on Landslides, Balkema, Rotterdam, 1843–1848.

Forgy, E. W.,1965. Cluster analysis of multivariate data: efficiency vs interpretability of classifications. Biometrics 21, 768–769.

Gupta RP., Joshi BC., 1990. Landslide hazard zonation using the GIS approach – a case study from the Ramganga Catchment, Himalayas. Eng Geol 28:119–131.

Guzzetti F, Carrara A, Cardinali M, Reichenbach P., 1999, Landslide hazard evaluation: a review of current techniques and their application in a multi-scale study, Central Italy. Geomorphology 31:181–216

Hansen, A., 1984. Landslide hazard analysis. In Brunsden, D. and Prior, D. B. (Eds.), Slope Instability, John Wiley and Sons, Chichester, 523–602.

Hutchinson, J. N., 1995. Landslide hazard assessment, keynote paper. In Bell (Ed.), Landslides, Proceedings of the 6th International Symposium on Landslides, Balkema, Rotterdam, 1805–1841.

Lee S, Choi J, Min K., 2002. Landslide susceptibility analysis and verification using the Bayesian probability model. Environ Geol 43:120–131.

Ozdemir, H., 2007. GIS and RS based Flood and Landslide Risk Analysis in the Havran River Basin (Balikesir), Istanbul University Social Science Enstitute, Unpublished Ph.D. Thesis, Istanbul.

Soeters R, van Westen CJ., 1996. Slope instability recognition, analysis, and zonation. In: Turner AK, Schuster RL (eds) Landslides: investigation and mitigation. Transport Res Board Spec Rep 247, pp 129–177

Suzen, M.L., and Toprak, V., 1998. Filtering of Satellite Images in Geological Lineament Analysis: An Application to Fault Zone in Central Turkey, International Journal of Remote Sensing, 19, pp. 1101-1114.

Van Westen CJ., 1997. Statistical landslide hazard analysis. In: Application guide, ILWIS 2.1 for Windows. ITC, Enschede, The Netherlands, pp 73–84

Varnes, D. J., 1984. Landslide hazard zonation: a review of principles and practice. UNESCO, Paris.

Voldati, T., 1995. Multiple-sources Remotely Sensed data for Lithological and Structural Mapping, ITC Journal, 2, pp. 95-113.

Yin, K.L., Yan, T.Z., 1988. Statistical prediction model for slope instability of metamorphosed rocks. In: Bonnard, C. (Ed.), Proc. 5th Int. Sym. on Landslides, Lausanne. Balkema, Rotterdam, pp. 1269– 1272.

Zezere, J.L., Reis, E., Garcia, R., Olieira, S., Rodrigues, M.L., Vieira, G., and Ferreira, A.B., 2004. Integration of spatial and temporal data for the definition of different landslide hazard scenarios in the area north of Lisbon (Portugal), Natural Hazards and Earth System Science, 4: 133-146.